RSC Advances

PAPER

View Article Online
View Journal | View Issue

Cite this: *RSC Adv.*, 2019, **9**, 30406

A single-phase white light emitting phosphor $Ba_3Y(PO_4)_3:Ce^{3+}/Tb^{3+}/Mn^{2+}$: luminescence, energy transfer and thermal stability

Yun Chen, Wenge Ding,* Panlai Li,* Xue Li, Qi Bao, Jinjin Liu, Keliang Qiu, Xiangyu Meng, Zhiping Yang and Zhijun Wang*

Received 2nd August 2019
Accepted 16th September 2019

DOI: 10.1039/c9ra05995d

rsc.li/rsc-advances

A series of Ce^{3+}/Tb^{3+}, Tb^{3+}/Mn^{2+} and $Ce^{3+}/Tb^{3+}/Mn^{2+}$ doped $Ba_3Y(PO_4)_3$ were synthesized by the high temperature solid state method. Phase formation, energy transfer, luminescence properties and thermal quenching properties of phosphors were analyzed in detail. For the co-doped samples, the energy transfer from Ce^{3+} to Tb^{3+} and Tb^{3+} to Mn^{2+} was proved by analyzing the spectra and fluorescence lifetime, and the energy transfer mechanism was calculated to be dipole–dipole interaction. A series of color-tunable phosphors were obtained by the energy transfer from Ce^{3+} to Tb^{3+} and Tb^{3+} to Mn^{2+}. For the tri-doped samples, it was confirmed that the energy transfers from Ce^{3+} to Tb^{3+}, Tb^{3+} to Mn^{2+} and Ce^{3+} to Mn^{2+} exist at the same time by analyzing the spectra properties, and it can emit warm-white light with extensive color temperature regulability. In addition, the thermal stability was abnormal and outstanding because the defects exist in the samples. The results show that the phosphors may be novel warm white emitting phosphors for white light emitting diodes.

1 Introduction

In recent years, white-light-emitting diodes (LEDs) have received more and more attention for their many advantages[1] Compared with traditional light sources, white LEDs have higher efficiency, higher brightness, longer service time and are more environmentally friendly, hence they are considered as the fourth generation light source.[1–7] The most common method to synthesize white LEDs is to combine the GaN blue LED chip with yellow phosphor YAG:Ce^{3+}. However, this type of white LED has many drawbacks due to lack of a red ingredient, such as the poor color rendering index and the high correlated color temperature.[3,4,8] Because white LEDs can not only be used in lighting field, but also in display and medical fields, hence they should show specific optical performance in different application scenarios which means that phosphors with high tunability are needed.[7,9] Nowadays, the ultraviolet-excited single-phased phosphors have been taken seriously, which can achieve white light with good color rendering index, suitable correlated color temperature and tunable emission by adjusting the doping ratio of different ions.[10–13] Therefore, it is urgent to find novel and high performance single-phased phosphors. Generally, when doping rare earth ions or transition metal ions into compound, the white emitting phosphor may be achieved by the energy transfer between different activator ions,[14] such as $Ca_{10}Na(PO_4)_7:Ce^{3+}/Tb^{3+}/Mn^{2+}$,[15] $Na_2Ba_6(Si_2O_7)(SiO_4)_2:Ce^{3+}/Eu^{2+}/Tb^{3+}/Mn^{2+}$.[16] Among many host compounds, the eulytite-type orthophosphates with the type of $M_3^{I}M^{II}(PO_4)_3$ (M^{I} = Ba, Sr, Ca, and Pb, M^{II} = La, Sc, Y, Bi, and In) have attracted great interests, for example, when doped Ce^{3+}, Tb^{3+}, and Mn^{2+} in $Ba_3Y(PO_4)_3$ (BYP), the phosphors can produce blue, green and red light, respectively.[17–19] Thus, it is possible to achieve white emission when the above three ions are tri-doped in BYP. Moreover, the thermal stability of phosphor is an essential characteristic. It has been reported in our previous work that BYP:Ce^{3+},Mn^{2+} shows extraordinary thermal stability due to the existence of defect in the samples.[17] It is expectable that the defect is to be utilized to gain a series of phosphors with high temperature stability in $Ce^{3+}/Tb^{3+}/Mn^{2+}$ doped BYP. In this work, series of Ce^{3+}/Tb^{3+}, Tb^{3+}/Mn^{2+} or $Ce^{3+}/Tb^{3+}/Mn^{2+}$ doped BYP are obtained. Phase formation, energy transfer, luminescence properties and thermal property were investigated in detail. Finally, series of single-phased white emitting phosphors are obtained by the energy transfer $Ce^{3+} \rightarrow Tb^{3+}$, $Tb^{3+} \rightarrow Mn^{2+}$ and $Ce^{3+} \rightarrow Mn^{2+}$.

2 Experimental

2.1 Sample preparation

Series of $Ba_3Y_{0.95-x}(PO_4)_3:0.05Ce^{3+},xTb^{3+}$, $Ba_{3-y}Y_{0.95}(PO_4)_3:0.05Ce^{3+},yMn^{2+}$ and $Ba_{2.86}Y_{0.7-z}(PO_4)_3:zCe^{3+},0.3Tb^{3+},0.14Mn^{2+}$ were synthesized by a high temperature solid state method. Raw materials $BaCO_3$

National-Local Joint Engineering Laboratory of New Energy Photoelectric Devices, Hebei Key Laboratory of Optic-electronic Information and Materials, College of Physics Science & Technology, Hebei University, Baoding 071002, China. E-mail: dwg@hbu.edu.cn; li_panlai@126.com; wangzj1998@126.com

(analytical reagents, A.R.), $NH_4H_2(PO_4)_3$ (A.R.), Y_2O_3 (99.99%), CeO_2 (99.99%), Tb_4O_7 (99.99%) and $MnCO_3$ (A.R.) were weighed according to stoichiometric proportions, and then mixed them in an agate mortar pestling for 20 min to ensure the materials are distributed uniformly. The mixed materials were put into crucibles and heated at 1300 °C for 3 h in a carbon reducing atmosphere. After firing, the samples cooled to room temperature slowly and were grounded into powder for subsequent use.

2.2 Materials characterization

XRD patterns of sample are measured by powder X-ray diffraction (XRD) using a D8-A25 Focus diffractometer at 40 kV and 40 mA with step size of 0.05° and a scan speed 0.1 s per step. Spectral property of sample was measured by Hitachi F-4600 fluorescence spectrophotometer with a 450 W Xe lamp as the excitation source. Decay curves were measured by Horiba FL-4600 fluorescence spectrophotometer with a 320 nm pulse laser radiation (nano-LED) for Ce^{3+} and 450 W Xe lamp as the excitation resource for Mn^{2+} at room temperature. Thermoluminescence spectra of samples were measured by a FJ-427A1 TL dosimeter at room temperature with a fixed heating rate of 1 k s^{-1} within the range 300–450 K. Commission Internationale de L'Eclairage (CIE) chromaticity coordinates of samples were obtained by the PMS-80 spectral analysis system.

3 Results and discussion

3.1 Phase formation

The XRD patterns of BYP:0.05Ce^{3+},$x$$Tb^{3+}$ (x = 0.02, 0.45), BYP:0.05Ce^{3+},$y$$Mn^{2+}$ (y = 0.08, 0.14) and BYP:$z$$Ce^{3+}$,0.3$Tb^{3+}$,0.14$Mn^{2+}$ (z = 0.07, 0.15) were shown in Fig. 1. It can be seen that no apparent impurity phase appears and all the diffraction peaks of samples can be indexed to the standard card of BYP (JCPDS No. 44-0318) appropriately. The XRD patterns illustrates that Ce^{3+}, Tb^{3+} and Mn^{2+} did not cause any significant change to the crystal structure of BYP and series of pure phase phosphors were obtained.

3.2 Luminescence and energy transfer properties of BYP:Ce^{3+},$x$$Tb^{3+}$

Fig. 2a–c display the emission and excitation spectra of BYP:0.05Ce^{3+} (λ_{ex} = 330 nm, λ_{em} = 400 nm), BYP:0.45Tb^{3+} (λ_{ex} = 377 nm, λ_{em} = 550 nm) and BYP:0.05Ce^{3+},0.15Tb^{3+} (λ_{ex} = 330 nm, λ_{em} = 400 nm, 550 nm), respectively. The emission spectrum of BYP:0.05Ce^{3+} shows a blue emission band peaking at 400 nm, which originates from the electron transition 5d → 4f of Ce^{3+}. The excitation band of BYP:0.05Ce^{3+} ranges from 200 nm to 360 nm (λ_{max} = 330 nm) due to the 4f → 5d electron transition. For BYP:0.45Tb^{3+}, a series of characteristic emission peaks of Tb^{3+} appear in the emission spectrum which originates from the electron transition $^5D_4 \rightarrow {}^7F_6$ (500 nm), $^5D_4 \rightarrow {}^7F_5$ (550 nm), $^5D_4 \rightarrow {}^7F_4$ (590 nm) and $^5D_4 \rightarrow {}^7F_3$ (630 nm) of Tb^{3+}, respectively. The excitation spectrum of BYP:0.45Tb^{3+} shows a broad excitation band from 210 nm to 400 nm because of the allowed $4f^8$–$4f^7$5d transition and intra-configuration transition of Tb^{3+}. Comparing the emission spectrum of BYP:0.05Ce^{3+} with the excitation spectrum of BYP:0.45Tb^{3+}, an obvious spectral overlapping can be observed which means an effective energy transfer from Ce^{3+} to Tb^{3+} (ET_{Ce-Tb}) may be occur.[19,20] In addition, the emission spectrum of BYP:0.05Ce^{3+},0.15Tb^{3+} contains both the emission band of Ce^{3+} and Tb^{3+}, the excitation spectrum monitored at 550 nm (emission peak of Tb^{3+}) has the similar profile with that monitored at 400 nm (emission peak of Ce^{3+}), it also means that there may be energy transfer from Ce^{3+} to Tb^{3+}.

In order to further investigate the luminescence properties, a series of BYP:Ce^{3+},$x$$Tb^{3+}$ were synthesized. Fig. 3a shows the emission spectra of BYP:0.05Ce^{3+},$x$$Tb^{3+}$ (x = 0–0.45) under 330 nm UV excitation. Fig. 3b reveals the emission intensity of Ce^{3+} (λ_{em} = 400 nm) and Tb^{3+} (λ_{em} = 550 nm), it can be seen that the emission intensity of Ce^{3+} declines constantly as the concentration of Tb^{3+} increasing, meanwhile, the emission intensity of Tb^{3+} goes up ceaselessly. According to the change of emission intensity, it means that an effective energy transfer from Ce^{3+} to Tb^{3+} is expectable.

To confirm the energy transfer from Ce^{3+} to Tb^{3+}, the decay curves of Ce^{3+} monitored at 400 nm under 320 nm pulse laser radiation (nano-LED) excitation and decay curves of Tb^{3+} monitored at 550 nm under 377 nm excitation for BYP:0.05Ce^{3+},$x$$Tb^{3+}$ are shown in Fig. 4a and b, respectively. The decay curves of Ce^{3+} and Eu^{2+} can be matched well with second-order exponential function, which can be expressed as the following expression:[21,22]

$$I_{(t)} = A_1 \exp(t/\tau_1) + A_2 \exp(t/\tau_2) \quad (1)$$

where $I_{(t)}$ is the luminescence intensity, A_1 and A_2 are constants, t is time, τ_1 and τ_2 are the lifetimes for the exponential components. The average lifetime τ^* can be calculated by the following formula[21,23]

$$\tau^* = (A_1\tau_1^2 + A_2\tau_2^2)/(A_1\tau_1 + A_2\tau_2) \quad (2)$$

The calculated average lifetime of Ce^{3+} and Tb^{3+} are shown in Fig. 4c, from which one can see that the lifetime of Ce^{3+} decreases consistently and that of Tb^{3+} increases consistently with increasing Tb^{3+} concentration. The lifetime can strongly prove the energy transfer from Ce^{3+} to Tb^{3+}, and the energy transfer efficiency can be calculated by the following equation[9,22]

$$\eta_T = 1 - \tau/\tau_0 \quad (3)$$

where τ and τ_0 are the decay time of the sensitizer Ce^{3+} in the presence and absence of activator Tb^{3+}, respectively. Fig. 4d shows that the energy transfer efficiency rises up constantly with increase Tb^{3+} concentration, and the maximum value is 69.9% when the doping concentration of Tb^{3+} reaches the maximum x = 0.45.

According to Dexter's theory, there are two types of interactions between sensitizers and activators: multipolar interaction and exchange interaction.[21,24] The critical distance between Ce^{3+} and Tb^{3+} (R_{Ce-Tb}) is a critical factor to judge which type it

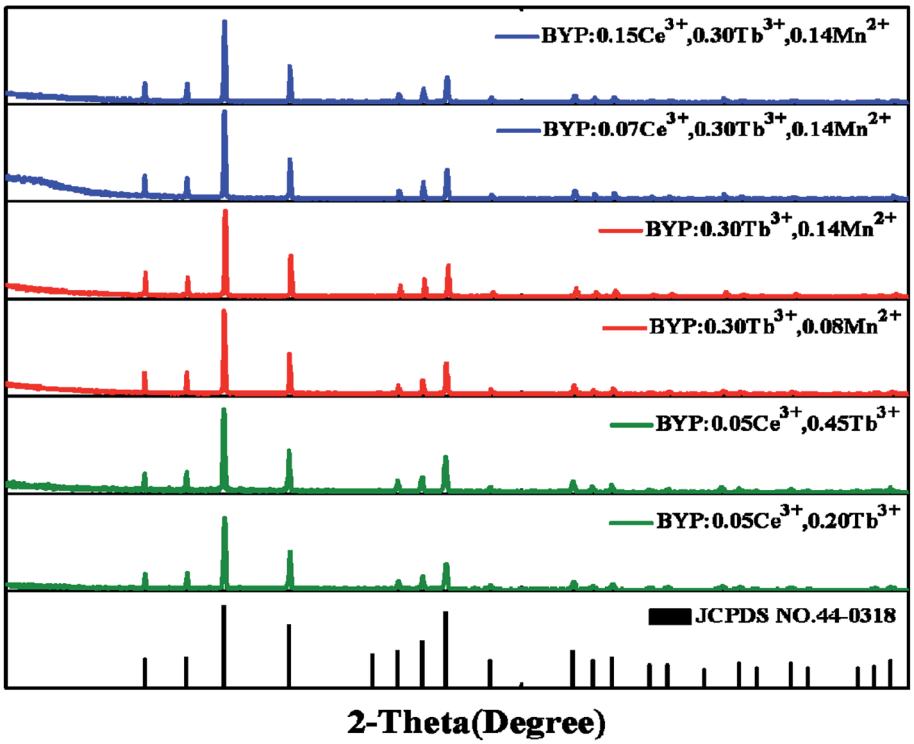

Fig. 1 XRD patterns of the representative samples and the standard patterns of $Ba_3Y(PO_4)_3$ (JCPDS No. 44-0318).

belongs to, and the critical distance R_{Ce-Tb} can be calculated by the following formula[25]

$$R_c = 2\left[\frac{3V}{4N\pi\chi_c}\right]^{\frac{1}{3}} \quad (4)$$

where N is the number of the cations in host, V is the volume of the unit cell. χ_c is the sum of Ce^{3+} and Tb^{3+} concentration when the emission intensity of Ce^{3+} in the presence of Tb^{3+} is half that in the absence of Tb^{3+}. Herein, V equals to 1165.61 Å^3 and N equals to 4, χ_c is calculated to be 0.2. Thus, the R_{Ce-Tb} is calculated to be 17.72 Å which is larger than the maximum distance of 5 Å for the exchange interaction, it means the energy

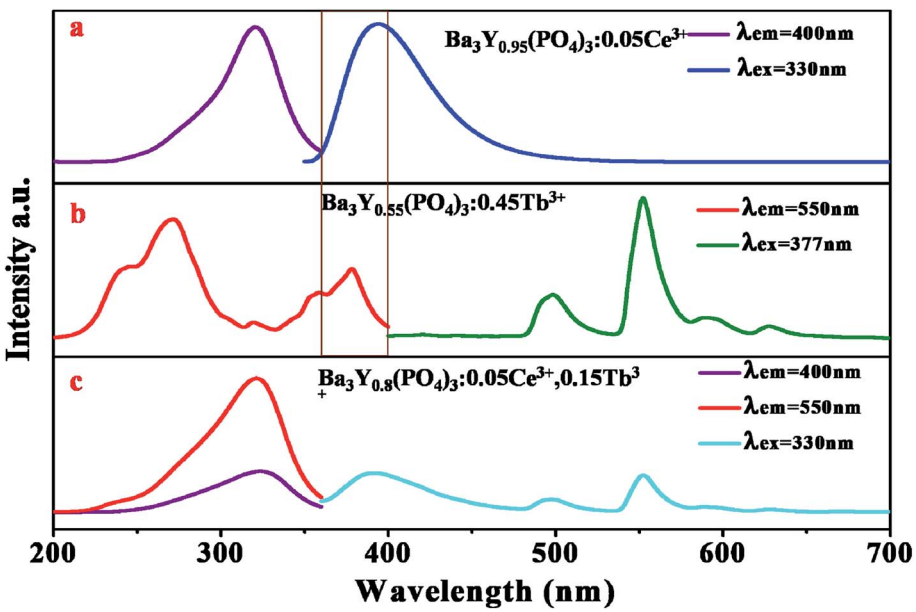

Fig. 2 Emission and excitation spectra of (a) BYP:0.05Ce^{3+}; (b) BYP:0.45Tb^{3+}; (c) BYP:0.05Ce^{3+},0.15Tb^{3+}.

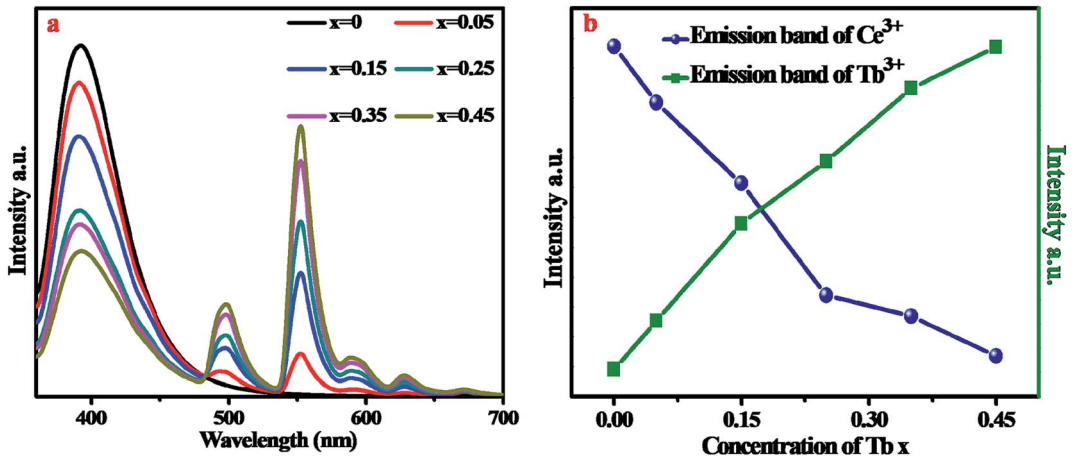

Fig. 3 (a) Emission spectra of BYP:0.05Ce^{3+},xTb^{3+} (x = 0–0.45). (b) Emission intensity of Ce^{3+} and Tb^{3+} as a function of Tb^{3+} concentration.

transfer mechanism of Ce^{3+}–Tb^{3+} belongs to multipolar interaction.

There are three kinds of multipolar interactions: dipole–dipole, dipole–quadrupole and quadrupole–quadrupole interaction. The mechanism of ET_{Ce-Tb} can be discussed by Dexter's theory:[24,26]

$$\frac{I_{s0}}{I_s} \propto C^{\frac{n}{3}} \quad (5)$$

where I_{s0} and I_s are the emission intensity of sensitizer Ce^{3+} in the absence and presence of the activator Tb^{3+}, respectively. The sum concentration of Ce^{3+} and Tb^{3+} is represented by C. Herein, n = 6, 8 and 10 correspond to dipole–dipole, dipole–quadrupole

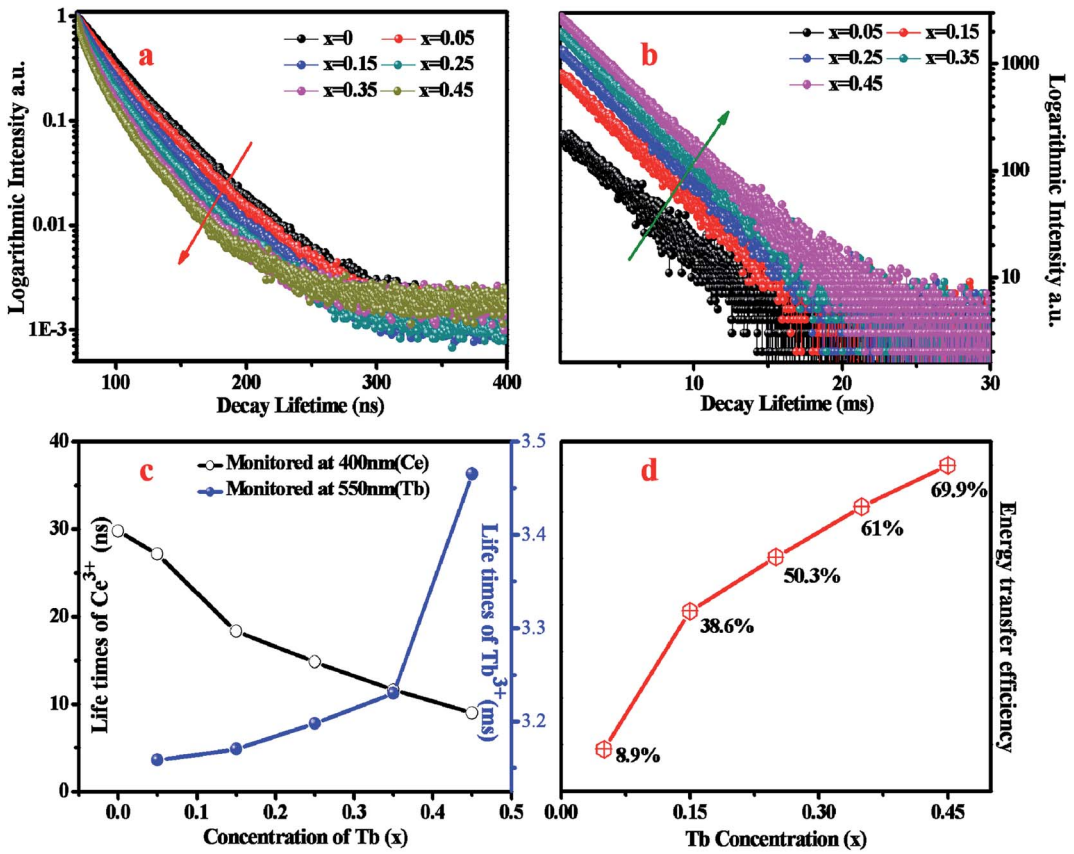

Fig. 4 (a) Decay curves of Ce^{3+} in BYP:0.05Ce^{3+},xTb^{3+} (λ_{em} = 400 nm, λ_{ex} = 320 nm). (b) Decay curves of Tb^{3+} in BYP:0.05Ce^{3+},xTb^{3+} (λ_{em} = 550 nm, λ_{ex} = 377 nm). (c) Lifetime of Ce^{3+} and Tb^{3+} as function of Tb^{3+} concentration. (d) Energy transfer efficiency from Ce^{3+} to Tb^{3+} as function of Tb^{3+} concentration.

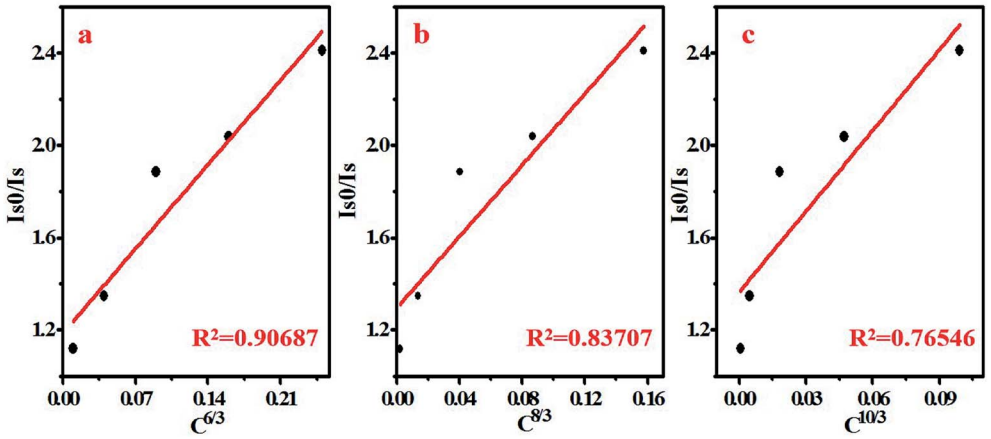

Fig. 5 Dependence of I_{s0}/I_s of Ce^{3+} and Tb^{3+} on $C^{6/3}$, $C^{8/3}$ and $C^{10/3}$ in BYP:0.05Ce^{3+},xTb^{3+}.

and quadrupole–quadrupole interactions, respectively.[24,26,27] The linear relationship between I_{s0}/I_s and $C^{n/3}$ for BYP:0.05Ce^{3+},xTb^{3+} are illustrated in Fig. 5, it can be seen that a well fitted curve can be gotten when $n = 6$ ($R^2 = 0.94952$), hence it can be concluded that the dipole–dipole interaction plays an essential role in the energy transfer from Ce^{3+} to Tb^{3+}.

The Commission Internationale de L'Eclairage (CIE) chromaticity coordinates of BYP:0.05Ce^{3+},xTb^{3+} (x = 0–0.45) was calculated basing on the relevant emission spectra under 330 nm excitation. The results along with luminescent photographs of related phosphors are depicted in Fig. 6, the emission color of BYP:0.05Ce^{3+},xTb^{3+} can be modulated from blue (0.1622, 0.0406) to yellow-green (0.2946, 0.4169). Hence, series of color-tunable phosphors were synthesized successfully.

To analyze the thermal stability of BYP:0.05Ce^{3+},xTb^{3+}, the temperature-dependent emission spectra of BYP:0.05Ce^{3+},0.45Tb^{3+} excited by 330 nm were measured which is shown in Fig. 7a, and the emission intensity of Ce^{3+} and Tb^{3+} with increasing the temperature is depicted in Fig. 7b. It can be seen from the pictures that the emission intensity of Ce^{3+} shows a first increases and then decreases with increasing the temperature, but it remains 107.7% of the initial value (300 K) when the temperature reaches 425 K. As for Tb^{3+}, its emission intensity increases constantly and reaches to 138.8% of the initial value when the temperature reaches 425 K. The abnormal change of emission intensity of Ce^{3+} and Tb^{3+} with temperature may be caused by the defects in BYP:0.05Ce^{3+},0.45Tb^{3+}.[28–30] Fig. 8a shows the thermoluminescence spectrum of BYP:0.05Ce^{3+},0.45Tb^{3+}, it can be seen that there are two emission bands ranging from 400 K to 420 K and from 460 K to 480 K, respectively. The thermoluminescence spectrum confirms the existence of defects. Fig. 8b depicts how defects affect the thermal stability of BYP:0.05Ce^{3+},xTb^{3+}: the shallow trap D1 and deep trap D2 can store the electrons, but the electrons transmit to the conduction band when BYP:0.05Ce^{3+},xTb^{3+} are heated. After that, a part of electrons transmit to $^5D_4$ energy level of Tb^{3+} and 5d energy band of Ce^{3+} from conduction band, then more

CIE chromaticity coordinates ofBYP:0.05Ce^{3+},xTb^{3+}	
x=0	(0.1622 , 0.0406)
x=0.05	(0.1909 , 0.1225)
x=0.15	(0.2352 , 0.2486)
x=0.25	(0.2677 , 0.3380)
x=0.35	(0.2838 , 0.3876)
x=0.45	(0.2946 , 0.4169)

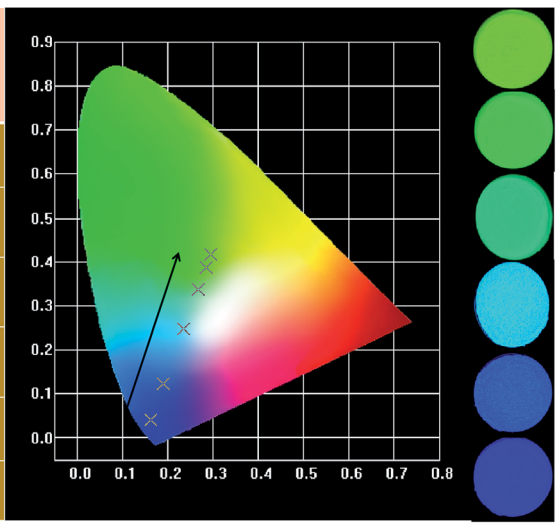

Fig. 6 CIE chromaticity coordinates of BYP:0.05Ce^{3+},xTb^{3+} (x = 0–0.45) along with their luminescent photographs.

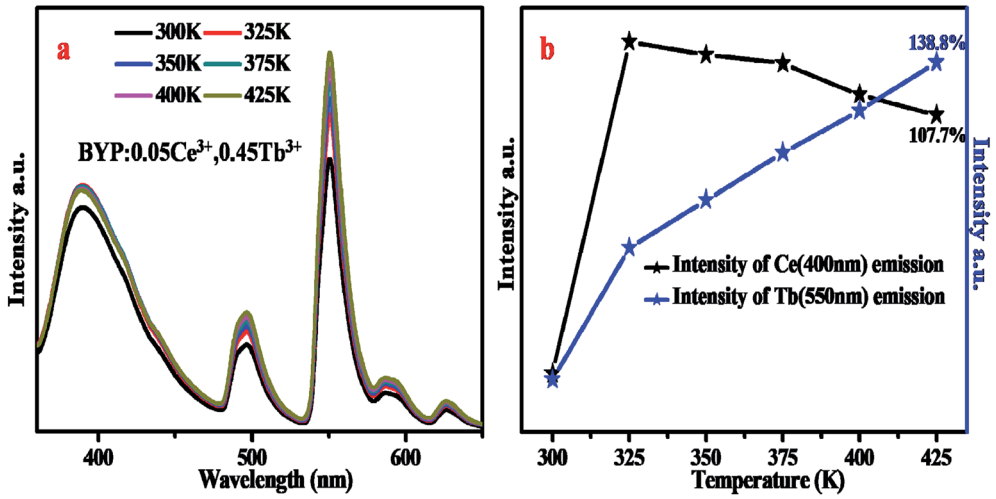

Fig. 7 (a) Temperature-dependent emission spectra of BYP:0.05Ce^{3+},xTb^{3+} excited by 330 nm. (b) Relative intensity of Ce^{3+} and Tb^{3+} in the temperature-dependent emission spectra.

electrons transmit from $^5D_4$ to ^7F_J energy level and 5d to 4f energy band by radiative transition meaning more energy would be released. Thus, the emission intensity of Ce^{3+} and Tb^{3+} rise up with increasing temperature.[29]

3.3 Luminescence and energy transfer of BYP:0.4Tb^{3+},yMn^{2+}

The emission spectra of BYP:0.4Tb^{3+},yMn^{2+} excited by 377 nm UV-light are shown in Fig. 9a and the relative emission intensities at 550 nm and 600 nm are depicted in Fig. 9b. The emission intensity of Tb^{3+} (550 nm) decreases constantly with increasing Mn^{2+} concentration, it means that Mn^{2+} may absorb energy from Tb^{3+}. It is worth noting that the emission peaks of Tb^{3+} and Mn^{2+} coexist at 600 nm, as increasing Mn^{2+} concentration the source of the peak at 600 nm change from Tb^{3+} ($^5D_4$–$^7F_4$) to both Mn^{2+} ($^4T_1$–$^6A_1$) and Tb^{3+} and Mn^{2+} is a main source. The intensity of the peak at 600 nm shows a first decrease, then increase and decrease in the end. The possible energy transfer maybe the main reason for the intensity changing: as increasing Mn^{2+} concentration the energy transfer from Tb^{3+} to Mn^{2+} started to work, thus the emission intensity shows a first decrease; after that, the concentration of Mn^{2+} is enough, hence the source of the emission peak mainly originates from Mn^{2+} and the emission intensity of Tb^{3+} is too low, thus the emission intensity of the peak at 600 nm started to pick up. In the end, the concentration of Mn^{2+} reaches the quenching point, so its emission intensity started to decrease again.

To confirm the energy transfer from Tb^{3+} to Mn^{2+} in BYP:0.4Tb^{3+},yMn^{2+}, the decay curves of Tb^{3+} (λ_{em} = 550 nm, λ_{ex} = 377 nm) and monitored at 600 nm (including Tb^{3+} and Mn^{2+}, λ_{ex} = 377 nm) are shown in Fig. 10a and b, respectively. The decay curves can be matched well with second-order exponential function expression (2), by means of expression (2) the

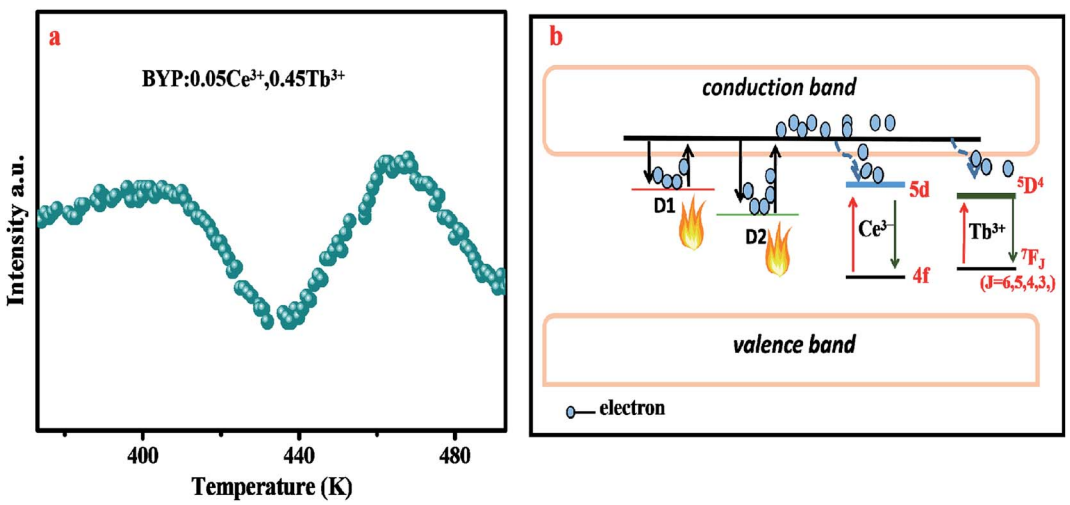

Fig. 8 (a) Thermoluminescence spectrum of BYP:0.05Ce^{3+},0.45Tb^{3+}. (b) Schematic diagram of the interaction between the defect and temperature-dependent emission intensity in BYP:0.05Ce^{3+},0.45Tb^{3+}.

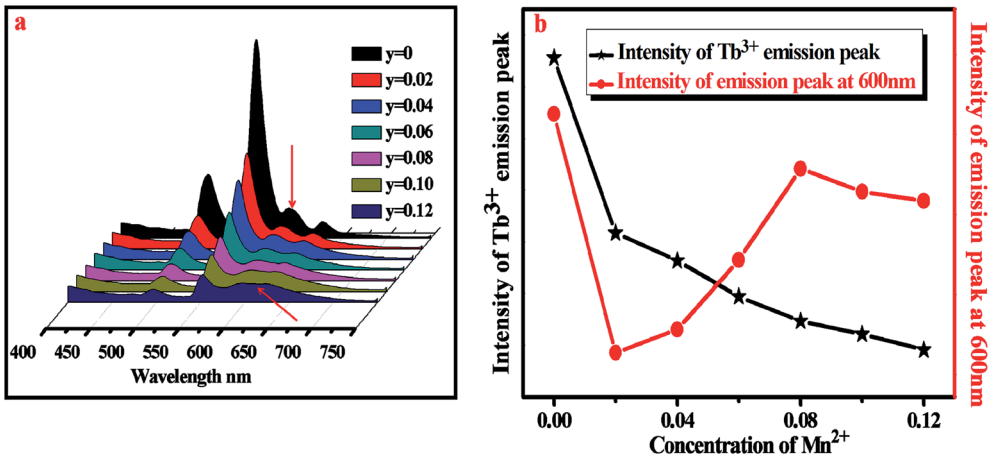

Fig. 9 (a) Emission spectra of BYP:0.4Tb^{3+},yMn^{2+} ($y = 0$–0.12). (b) Relative emission intensity at 550 nm and 600 nm.

average lifetimes can be calculated and the results are shown in Fig. 10c. It can be seen that the lifetime of Tb^{3+} decreases constantly as increasing Mn^{2+} concentration, this can prove the energy transfer from Tb^{3+} to Mn^{2+} (ET_{Ce-Tb}). In addition, the lifetime monitored at 600 nm shows a first decrease when $y = 0$ rises to $y = 0.02$, then increase when $y = 0.02$ rises to $y = 0.08$. This phenomenon is due to the low concentration of Mn^{2+} at the beginning, the measured and calculated lifetimes are mainly originated from Tb^{3+}, hence the lifetime decrease. When increased Mn^{2+} concentration, it passed into the lifetime of Mn^{2+}, thus the lifetime starts to increase.

The energy transfer efficiency of ET_{Tb-Mn} had been calculated by formula (3) and the results are shown in Fig. 10d. It can be seen that the energy transfer efficiency increases as Mn^{2+} concentration increasing and the maximum value is 52.3% when $y = 0.12$. The critical distance from Tb^{3+} to Mn^{2+} (Rc_{Tb-Mn})

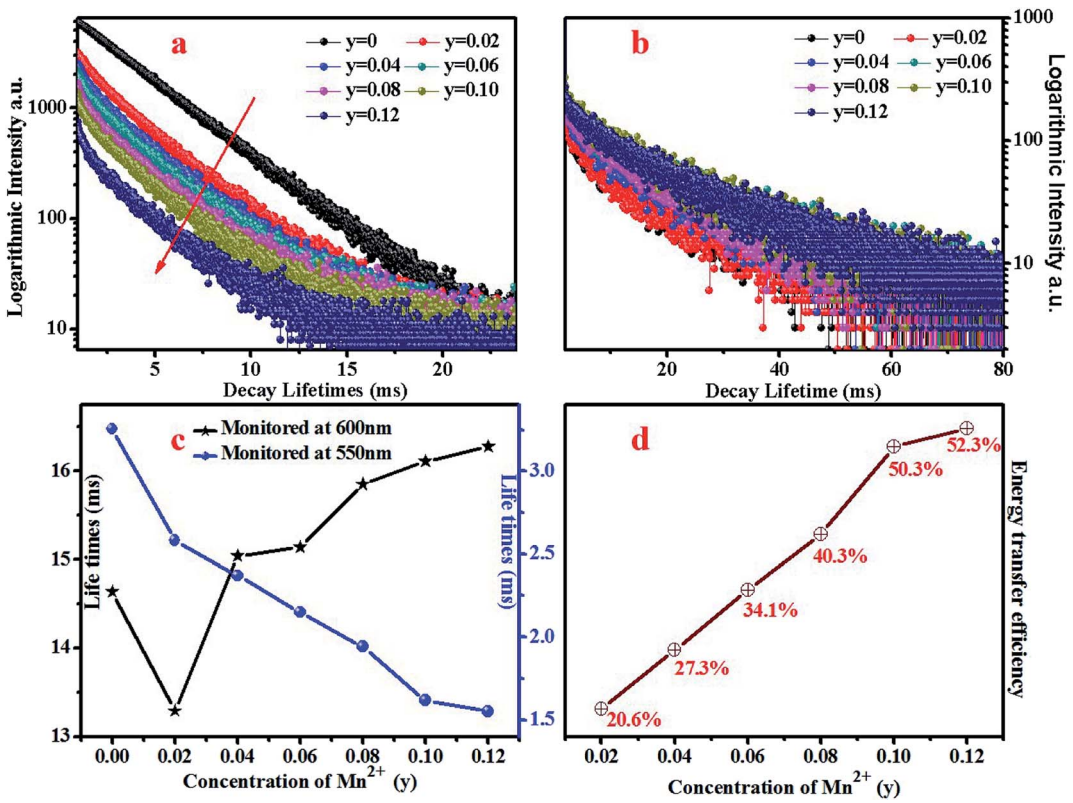

Fig. 10 (a) Decay curves of Tb^{3+} in BYP:0.4Tb^{3+},yMn^{2+} ($\lambda_{em} = 550$ nm, $\lambda_{ex} = 377$ nm). (b) Decay curves of Tb^{3+} and Mn^{2+} in BYP:0.4Tb^{3+},yMn^{2+} ($\lambda_{em} = 600$ nm, $\lambda_{ex} = 377$ nm). (c) Lifetime of Tb^{3+} and Mn^{2+} as function of Mn^{2+} concentration. (d) Energy transfer efficiency from Tb^{3+} to Mn^{2+} as function of Mn^{2+} concentration.

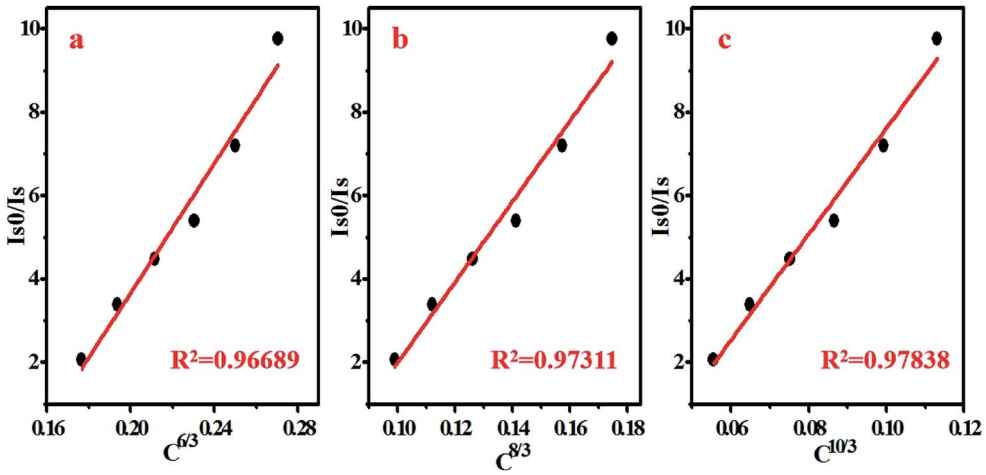

Fig. 11 Dependence of I_{s0}/I_s of Ce^{3+} and Tb^{3+} on $C^{6/3}$, $C^{8/3}$ and $C^{10/3}$ in BYP:0.4Tb^{3+},yMn^{2+}yMn^{2+}.

can be calculated by expression (4), for BYP:0.4Tb^{3+},yMn^{2+}, χ_c is calculated to be 0.42 and the Rc_{Tb-Mn} is calculated to be 13.84 Å which is obviously larger than the maximum distance of 5 Å for the exchange interaction. Thus it can be confirmed that the type of interaction between Tb^{3+} and Mn^{2+} is multipolar interaction. The linear relationship between I_0/I and $C^{n/3}$ for BYP:0.4Tb^{3+},yMn^{2+} are illustrated in Fig. 11a, and a well fitted curve can be gotten when $n = 10$ and $R^2 = 0.97838$, therefore, it can be confirmed that the ET_{Tb-Mn} mechanism is quadrupole–quadrupole interaction.

The Commission Internationale de L'Eclairage (CIE) chromaticity coordinates of BYP:0.4Tb^{3+},yMn^{2+} ($y = 0.02$–0.12) was calculated basing on the relevant emission spectra under 377 nm excitation. The calculated results along with luminescent photographs of related phosphors are depicted in Fig. 12, the emission color of BYP:0.4Tb^{3+},yMn^{2+} can be modulated from yellow-greenish (0.3329, 0.5275) to white (0.3936, 0.3562). Thus, BYP:0.4Tb^{3+},yMn^{2+} can act as a color-tunable material which can be used in near UV based white LEDs.

The temperature-dependent emission spectra of BYP:0.4Tb^{3+},0.12Mn^{2+} excited by 377 nm was measured and shown in Fig. 13a, and the emission intensity of Tb^{3+} and Mn^{2+} is presented in Fig. 13b. It can be seen from Fig. 13a that the emission peak of Mn^{2+} shifts from 600 nm to 588 nm due to the thermally active phonon-assisted excitation from lower energy levels to higher energy levels in the excited state of Mn^{2+}.[24] Because of the thermal quenching, the emission intensity of Mn^{2+} decreases continually with the increase of temperature and remains 80.5% of the initial value (300 K) when the temperature reaches 425 K. However, the emission intensity of Tb^{3+} increases continually, and when the temperature reaches 425 K the emission intensity rises to 111.6% of the initial value.

The abnormal change of emission intensity of Tb^{3+} is also caused by the defects in BYP:0.4Tb^{3+},0.12Mn^{2+}. Fig. 14a depicts the thermoluminescence spectrum of BYP:0.4Tb^{3+},0.12Mn^{2+}, as

CIE chromaticity coordinates of BYP:0.4Tb^{3+},yMn^{2+}	
y=0.02	(0.3329 , 0.5275)
y=0.04	(0.3518 , 0.4715)
y=0.06	(0.3700,0.4498)
y=0.08	(0.3747 , 0.4272)
y=0.10	(0.3944 , 0.3700)
y=0.12	(0.3936 , 0.3562)

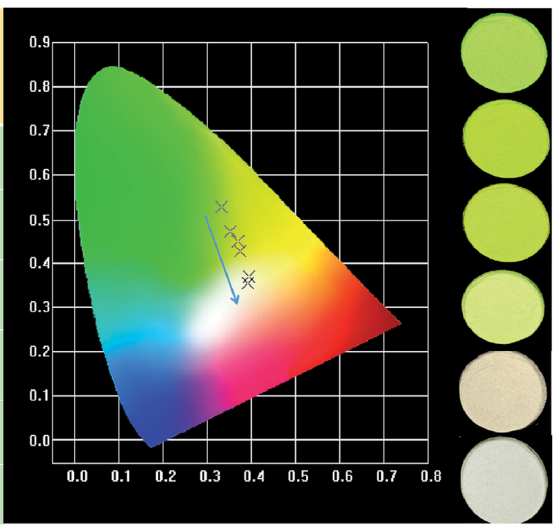

Fig. 12 CIE chromaticity coordinates of BYP:0.4Tb^{3+},yMn^{2+} ($y = 0.02$–0.12) along with their luminescent photographs.

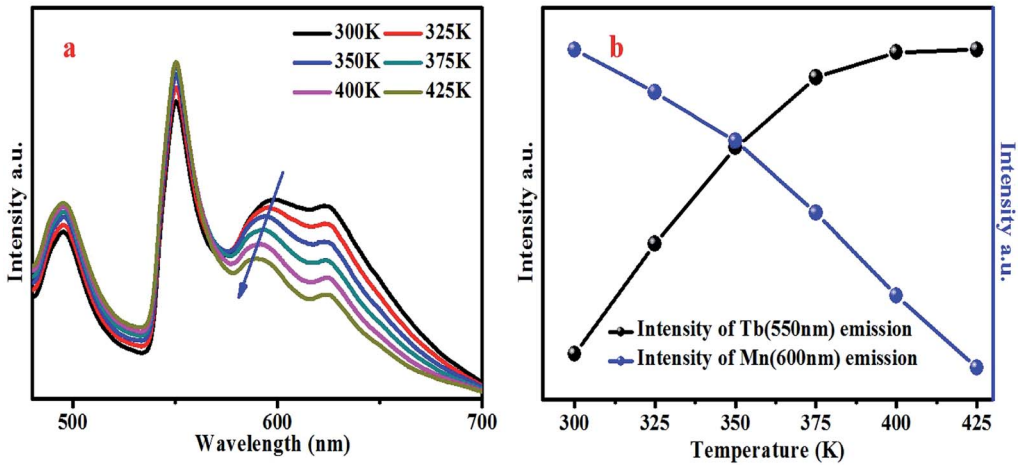

Fig. 13 (a) Temperature-dependent emission spectra of BYP:0.4Tb^{3+},0.12Mn^{2+} excited by 377 nm. (b) Relative intensity of Tb^{3+} and Mn^{2+} in the temperature-dependent emission spectra.

mentioned in Chapter 3.2: the emission intensity change of Ce^{3+} and Tb^{3+} in temperature-dependent emission spectra of BYP:0.05Ce^{3+},0.45Tb^{3+}. Fig. 14b is the schematic diagram on how the defects affect the emission intensity of Tb^{3+} in BYP:0.4Tb^{3+},0.12Mn^{2+}.

3.4 Luminescence and energy transfer of BYP:zCe^{3+},0.4Tb^{3+},0.12Mn^{2+}

Fig. 15a shows the emission spectra of BYP:0.15Ce^{3+},0.4Tb^{3+},0.12Mn^{2+} excited by 330 nm, it can be seen that the emission peaks of Ce^{3+} (390 nm), Tb^{3+} (550 nm) and Mn^{2+} (600 nm) coexist in the emission spectra covering blue, yellow, green and red region, thus, the efficient white emission is expectable. Fig. 15b depicts the excitation spectra of BYP:0.15Ce^{3+},0.4Tb^{3+},0.12Mn^{2+} monitored at 390 nm, 550 nm and 600 nm, from which one can see that the obtained three spectra have the similar profile, it means that there is energy transfer among Ce^{3+}, Tb^{3+} and Mn^{2+}. To further investigate the luminescence and energy transfer, the emission spectra of BYP:zCe^{3+},0.4Tb^{3+},0.12Mn^{2+} under 330 nm excitation are shown in Fig. 15c, the relative intensity of Ce^{3+}, Tb^{3+} and Mn^{2+} is depicted in Fig. 15d. It can be seen that the emission intensity of Ce^{3+}, Tb^{3+} and Mn^{2+} increase continuously with increasing Ce^{3+} concentration, it indicates that there are ET_{Ce-Tb}, ET_{Ce-Mn} and ET_{Tb-Mn} in BYP:zCe^{3+},0.4Tb^{3+},0.12Mn^{2+}.

Fig. 16 shows the Commission Internationale de L'Eclairage (CIE) chromaticity coordinates of BYP:zCe^{3+},0.4Tb^{3+},0.12Mn^{2+} (z = 0.01–0.11) and luminescent photographs of related phosphors when excited by 330 nm UV excitation. The emission color of BYP:zCe^{3+},0.4Tb^{3+},0.12Mn^{2+} can be modulated from white (0.3030 , 0.2893) with high color temperature to white (0.4096 , 0.3770) with low color temperature, *viz.*, a series of single-phased white light-emitting phosphors are realized successfully, and it maybe a potential application in white LEDs.

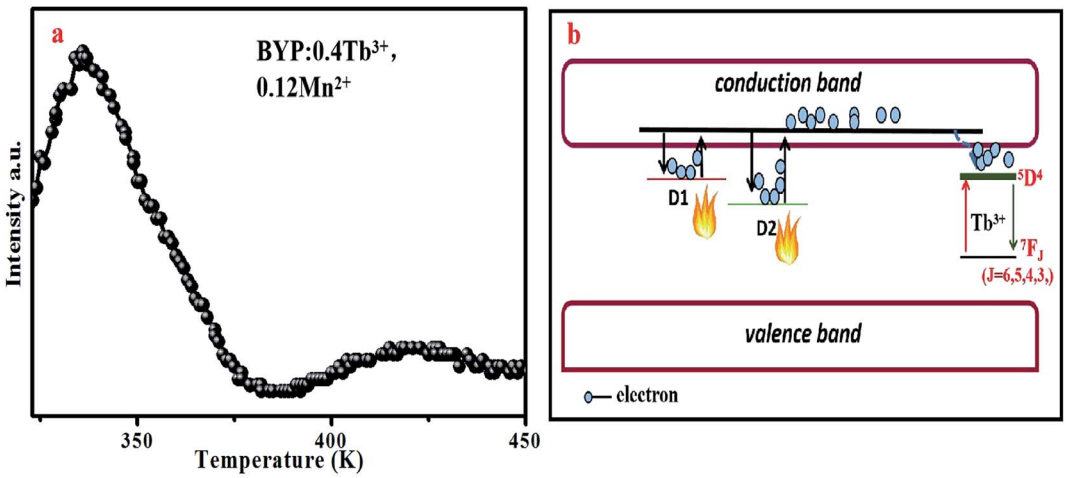

Fig. 14 (a) Thermoluminescence spectrum of BYP:0.4Tb^{3+},0.12Mn^{2+}. (b) Schematic diagram of the interaction between the defect and temperature-dependent emission intensity in BYP:0.4Tb^{3+},0.12Mn^{2+}.

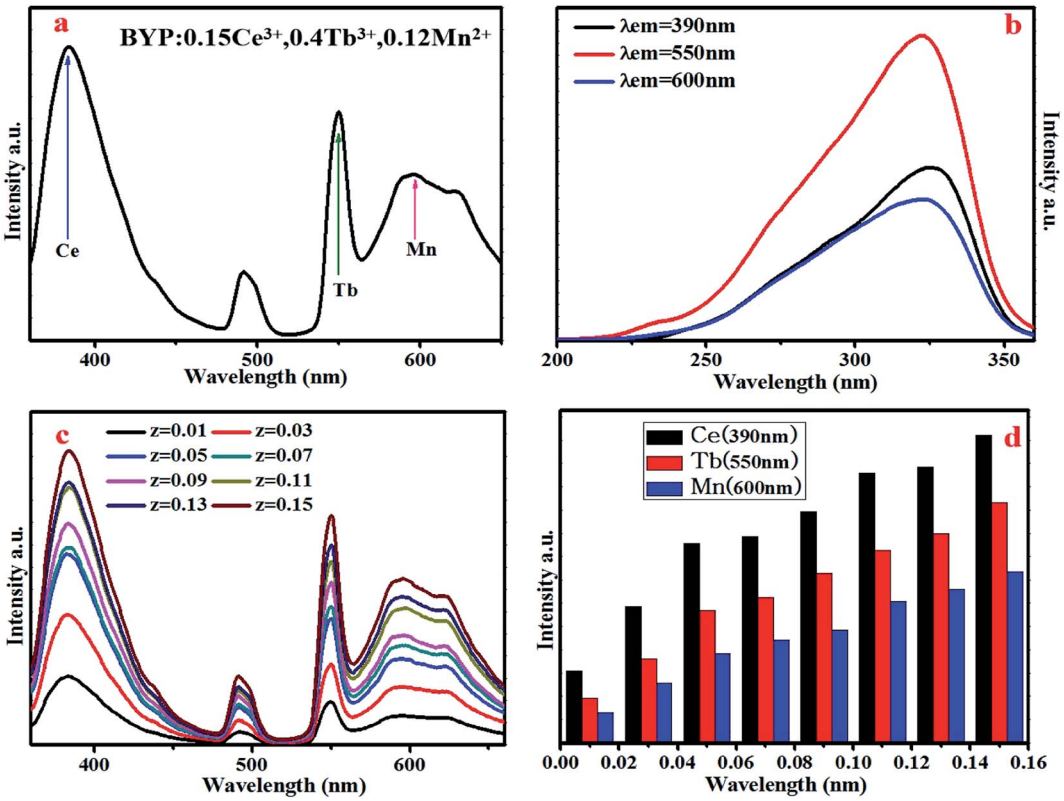

Fig. 15 (a) Emission spectrum of BYP:0.15Ce^{3+},0.4Tb^{3+},0.12Mn^{2+} (λ_{ex} = 330 nm). (b) Excitation spectra of BYP:0.15Ce^{3+},0.4Tb^{3+},0.12Mn^{2+} (λ_{em} = 390 nm, 550 nm and 600 nm). (c) Emission spectra of BYP:zCe^{3+},0.4Tb^{3+},0.12Mn^{2+} (λ_{ex} = 330 nm). (d) Relative intensity of Ce^{3+}, Tb^{3+} and Mn^{2+} in BYP:zCe^{3+},0.4Tb^{3+},0.12Mn^{2+}.

As a representative, BYP:0.03Ce^{3+},0.4Tb^{3+},0.12Mn^{2+} was chosen to explore the thermal stabilities. Fig. 17a depicts the temperature-dependent emission spectra of BYP:0.03Ce^{3+},0.4Tb^{3+},0.12Mn^{2+} under 330 nm UV excitation, Fig. 17b shows the emission intensity of Ce^{3+}, Tb^{3+} and Mn^{2+}. The emission peak of Mn^{2+} shifts from 600 nm to 587 nm with increasing the temperature and the reason is the same as that mentioned above, it is because of the thermally active phonon-assisted of Mn^{2+}. With rising of temperature, the emission intensity of Mn^{2+} decreases due to thermal quenching effect

CIE chromaticity coordinates of BYP: zCe^{3+}, 0.4Tb^{3+},0.12Mn^{2+}	
z=0.01	(0.3030 , 0.2893)
z=0.03	(0.3308 , 0.3083)
z=0.05	(0.3408, 0.3233)
z=0.07	(0.3651 , 0.3431)
z=0.09	(0.3837 , 0.3574)
z=0.11	(0.4096 , 0.3770)

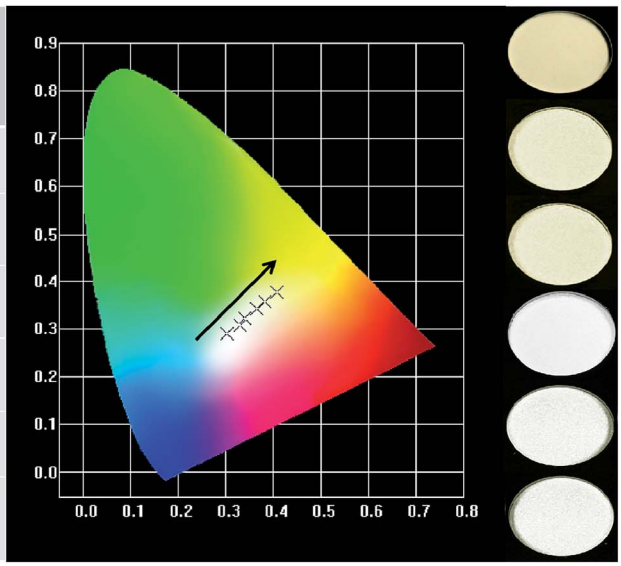

Fig. 16 CIE chromaticity coordinates of BYP:zCe^{3+},0.4Tb^{3+},0.12Mn^{2+} (z = 0.01–0.11) along with their luminescent photographs.

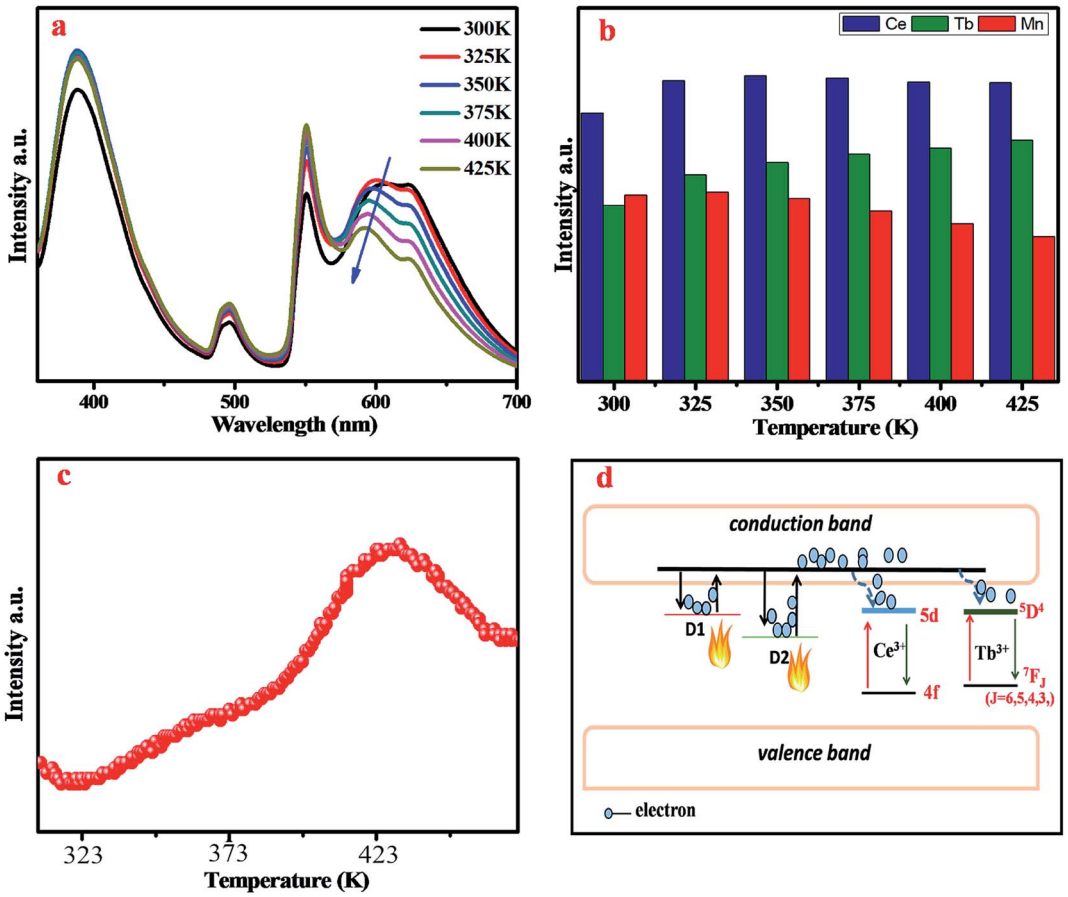

Fig. 17 (a) Temperature-dependent emission spectra of BYP:0.4Tb^{3+},0.12Mn^{2+} under 330 nm UV excitation. (b) Relative intensity of Ce^{3+}, Tb^{3+} and Mn^{2+}. (c) Thermoluminescence spectrum of BYP:0.03Ce^{3+},0.4Tb^{3+},0.12Mn^{2+}. (d) Schematic diagram of the interaction between the defect and temperature-dependent emission intensity in BYP:0.03Ce^{3+},0.4Tb^{3+},0.12Mn^{2+}.

and it still remains 80.8% of the initial value when the temperature rises to 425 K. The emission intensity of Ce^{3+} shows a first increase and then decrease, the emission intensity of Tb^{3+} increases constantly with increasing temperature. Fig. 17c presents the thermoluminescence spectrum of BYP:0.03Ce^{3+},0.4Tb^{3+},0.12Mn^{2+}. The change in emission intensity of Ce^{3+} and Tb^{3+} is ascribed to the same theory as mentioned in chapter 3.2: the emission intensity change of Ce^{3+} and Tb^{3+} in temperature-dependent emission spectra of BYP:0.05Ce^{3+},0.45Tb^{3+}. Fig. 17d is the schematic diagram on how the defects affect the emission intensity of Ce^{3+} and Tb^{3+} in BYP:0.03Ce^{3+},0.4Tb^{3+},0.12Mn^{2+}.

4 Conclusions

In summary, a series of eulytite-typed and single-phased phosphors BYP:0.05Ce^{3+}, $x$$Tb^{3+}$, BYP:0.05$Ce^{3+}$, $y$$Mn^{2+}$ and BYP:$z$$Ce^{3+}$,0.3$Tb^{3+}$,0.14$Mn^{2+}$ were synthesized successfully. The energy transfer from Ce^{3+} to Tb^{3+} and Tb^{3+} to Mn^{2+} were confirmed by analyzing its spectra and fluorescence lifetime. The thermal stability of samples is extraordinary, and it had been proved that the unusual temperature performance is caused by the defects in the samples. Finally, a series of single-phased color-tunable with high thermal stability phosphors were obtained, especially BYP:$z$$Ce^{3+}$,0.3$Tb^{3+}$,0.14$Mn^{2+}$, it can emit warm white light and the color temperature can be modulated by the energy among Ce^{3+}, Tb^{3+} and Mn^{2+}. Thus, it may have application potential in white LEDs.

Conflicts of interest

There are no conflicts to declare.

Acknowledgements

The work is supported by the National Natural Science Foundation of China (Nos. 51672066, 51902080), the Funds for Distinguished Young Scientists of Hebei Province, China (No. A2018201101), and the Natural Science Foundation of Hebei Province, China (No. E2019201223).

References

1 J. W. Qiao, Z. Zhao, Q. L. Liu and Z. G. Xia, Recent advances in solid-state LED phosphors with thermally stable luminescence, *J. Rare Earths*, 2019, **37**, 565–572.

2 C. Li, H. W. Zheng, H. W. Wei, S. J. Qiu, L. Xu, X. M. Wang and H. Jiao, Color tunable and white light emitting $Ca_2Si_5N_8$:Ce^{3+}, Eu^{2+} phosphor via efficient energy transfer for near-UV white LEDs, *Dalton Trans.*, 2018, **47**(19), 6860–6867.

3 F. B. Xiong, S. X. Liu, H. F. Lin, X. G. Meng, S. Y. Lian and W. Z. Zhu, A novel white-light-emission phosphor Dy^{3+}-doped $CaLaB_7O_{13}$ under UV excitation, *Opt. Laser Technol.*, 2018, **106**, 29–33.

4 M. Zhao, H. Liao, M. S. Molokeev, Y. Zhou, Q. Zhang, Q. Liu and Z. Xia, Emerging ultra-narrow-band cyan-emitting phosphor for white LEDs with enhanced color rendition, *Light: Sci. Appl.*, 2019, **8**, 38.

5 X. Y. Huang and H. Guo, $LiCa_3MgV_3O_{12}$:Sm^{3+}: A new high-efficiency white-emitting phosphor, *Ceram. Int.*, 2018, **44**, 10340–10344.

6 N. T. K. Chi, N. T. Tuan, N. T. K. Lien and H. Nguyen, Red Emission of $SrAl_2O_4$:Mn^{4+} Phosphor for Warm White Light-Emitting Diodes, *J. Electron. Mater.*, 2018, (10), 1–8.

7 J. X. Hu, T. H. Huang, Y. P. Zhang, B. Lu, H. Q. Ye, B. J. Chen, H. P. Xia and C. Y. Ji, Enhanced deep-red emission from Mn^{4+}/Mg^{2+} co-doped $CaGdAlO_4$ phosphors for plant cultivation, *Dalton Trans.*, 2019, **48**, 2455–2466.

8 J. T. Zhao, X. Y. Sun and Z. Q. Wang, Ce^{3+}/Eu^{2+} doped $SrSc_2O_4$ phosphors: Synthesis, luminescence and energy transfer from Ce^{3+} to Eu^{2+}, *Chem. Phys. Lett.*, 2018, **691**, 68–72.

9 Z. Y. Mao, J. J. Chen, J. Li and D. J. Wang, Dual-responsive Sr_2SiO_4:Eu^{2+}-$Ba_3MgSi_2O_8$:Eu^{2+},Mn^{2+} composite phosphor to human eyes and plant chlorophylls applications for general lighting and plant lighting, *Chem. Eng. J.*, 2016, **284**, 1003–1007.

10 S. Wang, Y. F. Li, L. G. Feng, L. Z. Zhang, Y. Zhang, X. L. Su, W. Ding and F. Yun, Laser patterning of $Y_3Al_5O_{12}$:Ce^{3+} ceramic phosphor platelets for enhanced forward light extraction and angular color uniformity of white LEDs, *Opt. Express*, 2016, **24**(15), 17522–17531.

11 Y. Zhang, X. J. Zhang, H. R. Zhang, L. L. Zheng, Y. Zeng, Y. Lin, Y. L. Liu and B. F. Lei, Tunable emission from green to red in the $GdSr_2AlO_5$:Tb^{3+},Eu^{3+}phosphor via efficient energy transfer, *RSC Adv.*, 2018, **8**(7), 3530–3535.

12 T. Senden, E. J. V. Harten and A. Meijerink, Synthesis and narrow red luminescence of Cs_2HfF_6:Mn^{4+} a new phosphor for warm white LEDs, *J. Lumin.*, 2018, **194**, 131–138.

13 H. P. You, Y. H. Song, G. Jia and G. Y. Hong, Energy transfer from Tb^{3+} to Mn^{2+} in $LaMgAl_{11}O_{19}$:Tb, Mn phosphors, *Opt. Mater.*, 2008, **31**(2), 342–345.

14 Z. M. Zhao, Z. G. Xia, X. X. Huang, L. X. Ning, G. Romain, M. S. Molokeev, Y. Y. Zhou, Y. C. Chuang, Q. Y. Zhang, Q. L. Liu and K. R. Poeppelmeier, Li substituent tuning of LED phosphors with enhanced efficiency, tunable photoluminescence, and improved thermal stability, *Sci. Adv.*, 2019, **5**, eaav0363.

15 J. R. Sun, P. Huang, Y. F. Liu, L. Wang, C. E. Cui, Q. F. Shi and Y. Tian, Color-tunable $Ca_{10}Na(PO_4)_7$:Ce^{3+}/Tb^{3+}/Mn^{2+}, phosphor via energy transfer, *J. Rare Earths*, 2018, **36**(6), 567–574.

16 W. Lü, H. W. Xu, M. M. Hao, H. C. Wang and X. J. Kang, Tunable full-color emitting $Na_2Ba_6(Si_2O_7)(SiO_4)_2$:$Ce^{3+}$, Eu^{2+}, Tb^{3+}, Mn^{2+}, phosphor for UV white LEDs: Photoluminescence and energy transfer, *J. Alloys Compd.*, 2018, **752**, 231–237.

17 Y. Chen, Z. J. Wang, W. G. Ding, X. Li, Q. Bao, J. J. Liu, K. L. Qiu, X. Y. Meng, Z. P. Yang and P. L. Li, A single-phase white light emitting phosphor $Ba_3Y(PO_4)_3$:Ce^{3+}/Eu^{2+}/Mn^{2+}: Luminescence, energy transfer and thermal stability, *J. Lumin.*, 2019, **210**, 322–334.

18 C. H. Huang, T. W. Kuo and T. M. Chen, Thermally stable green $Ba_3Y(PO_4)_3$:Ce^{3+},Tb^{3+} and red $Ca_3YAlO_3(BO_3)_4$:Eu^{3+} phosphors for white-light fluorescent lamps, *Opt. Express*, 2011, **19**(S1), A1–A6.

19 N. Guo, C. Z. Jia, J. Li, Y. F. Zhao, R. Z. Oyang and W. Lü, Color Tuning and Energy Transfer in Eu^{2+}/Mn^{2+}-Doped $Ba_3Y(PO_4)_3$ Eulytite-Type Orthophosphate Phosphors, *RSC Adv.*, 2015, **5**(58), 46517–46524.

20 Y. B. Chen, K. W. Cheah and M. L. Gong, Low thermal quenching and high-efficiency Ce^{3+}, Tb^{3+}-co-doped $Ca_3Sc_2Si_3O_{12}$ green phosphor for white light-emitting diodes, *J. Lumin.*, 2011, **131**(8), 1589–1593.

21 C. Wang, P. L. Li, Z. J. Wang, Z. P. Yang, Z. L. Li, M. M. Tian, J. G. Cheng and Y. S. Sun, Crystal structure, luminescence properties, energy transfer and thermal properties of a novel color-tunable, white light-emitting phosphor $Ca_{9-x-y}Ce(PO_4)_7$:xEu^{2+},yMn^{2+}, *Phys. Chem. Chem. Phys.*, 2016, **18**(41), 28661–28673.

22 S. C. Xu, Z. J. Wang, P. L. Li, T. Li, Q. Y. Bai, J. Sun and Z. P. Yang, White-emitting phosphor $Ba_2B_2O_5$:Ce^{3+}, Tb^{3+}, Sm^{3+}: luminescence, energy transfer, and thermal stability, *J. Am. Ceram. Soc.*, 2017, **100**, 2069–2080.

23 X. Li, P. L. Li, Z. J. Wang, S. M. Liu, Q. Bao, X. Y. Meng and K. L. Qiu, Color-tunable luminescence properties of Bi^{3+} in $Ca_5(BO_3)_3F$ via changing site occupation and energy transfer, *Chem. Mater.*, 2017, **29**(20), 8792–8803.

24 X. G. Zhang, J. G. Xu and M. L. Gong, Site-occupancy, luminescent properties and energy transfer of a violet-to-red color-tunable phosphor $Ca_{10}Li(PO_4)_7$:Ce^{3+}, Mn^{2+}, *J. Lumin.*, 2017, **183**, 348–354.

25 Y. Zhang, X. J. Zhang, H. R. Zhang, L. L. Zheng, Y. Zeng, Y. Lin, Y. L. Liu and B. F. Lei, Tunable emission from green to red in the $GdSr_2AlO_5$:Tb^{3+}, Eu^{3+} phosphor via efficient energy transfer, *RSC Adv.*, 2018, **8**, 3530–3535.

26 G. G. Li, Y. Tian, Y. Zhao and J. Lin, Recent progress in luminescence tuning of Ce^{3+} and Eu^{2+}-activated phosphors for pc-WLEDs, *Chem. Soc. Rev.*, 2016, **47**(1), 8688–8713.

27 F. Xiao, R. X. Yi, H. L. Yuan, G. J. Zang and C. N. Xie, Color tunable emission and energy transfer of Ce^{3+}/Dy^{3+} codoped $Ba_3La_2(BO_3)_4$ phosphor for UV white LEDs, *Spectrochim. Acta, Part A*, 2018, **202**, 352–358.

28 H. J. Guo, Y. T. Wang, G. Li, J. Liu, P. Feng and D. W. Liu, Cyan emissive super-persistent luminescence and thermoluminescence in $BaZrSi_3O_9$:Eu^{2+}, Pr^{3+} phosphors, *J. Mater. Chem. C*, 2017, **5**(11), 2844–2851.

29 Z. L. Li, Z. J. Wang, P. L. Li, J. G. Cheng, M. M. Tian, C. Wang and Z. P. Yang, Improvement of thermally stable and photoluminescence in $Sr_{0.8}Ca_{0.2}Al_2Si_2O_8:Eu^{2+}$ by the substitution of Si-Na # Al-Sr and Ca # Sr on structural modifications, *Dalton Trans.*, 2017, **41**, 14310–14317.

30 Q. Y. Bai, Z. J. Wang, P. L. Li, S. C. Xu, T. Li, J. G. Cheng and Z. P. Yang, Utilizing Tb^{3+} as the energy transfer bridge to connect Eu^{3+}-Zn2GeO4 host: Realization of efficient Eu^{3+} red emission, *Mater. Des.*, 2016, **108**, 597–607.